Energy Conversion and Management 291 (2023) 117259

Contents lists available at ScienceDirect

Energy Conversion and Management

journal homepage: www.elsevier.com/locate/enconman

Study on hydrogen substitution in a compressed natural gas spark-ignition passenger car engine

S. Molina, R. Novella, J. Gomez-Soriano *, M. Olcina-Girona

CMT – Motores Térmicos, Universitat Politècnica de València, Camino de Vera s/n, 46022 Valencia, Spain

ARTICLE INFO

Keywords:
Hydrogen
Compressed natural gas
HCNG blends
Decarbonization
Dual-fuel
Spark-ignition engine

ABSTRACT

Hydrogen substitution in applications fueled by compressed natural gas arises as a potential alternative to fossil fuels, and it may be the key to an effective hydrogen economy transition. The reduction of greenhouse gas emissions, especially carbon dioxide and unburned methane, as hydrogen is used in transport and industry applications, makes its use an attractive option for a sustainable future. The purpose of this research is to examine the gradual adoption of hydrogen as a fuel for light-duty transportation. Particularly, the study focuses on evaluating the performance and emissions of a single-cylinder port fuel injection spark-ignition engine as hydrogen is progressively increased in the natural gas-based fuel blend. Results identify the optimal conditions for air dilution and engine operation parameters to achieve the best performance. They corroborate that the dilution rate has to be adjusted to control pollutant emissions as the percentage of hydrogen is increased. Moreover, the study identifies the threshold for hydrogen substitution below which the reduction of carbon dioxide emissions due to efficiency gains is negligible compared to the reduction of the carbon content in the fuel blend. These findings will help reduce the environmental footprint of light-duty transportation not only in the long term but also in the short and medium terms.

1. Introduction

Concentrations of carbon dioxide (CO_2), methane (CH_4), and dinitrogen oxide (N_2O) in the atmosphere have reached the highest values recorded to date. The increase of these greenhouse gases (GHG) compared to the most pessimistic predictions suggests that the harmful consequences of global warming will increase in the medium and also in the short term. Historical records evince a significant global surface temperature increment since 1970 [1]. As a consequence, the temperature increase threshold established at the Paris Climate Conference (COP21) [2], will be exceeded if no drastic measures to reduce GHG emissions are taken in the next few years.

Around 73.2% of worldwide GHG emissions are related to energy production. This percentage considers the contribution of transportation (including road, rail, air, and marine applications), which represents 16.2% of the total. The global road transport emissions account for 11.9% [3], whereas this value increases 19.4% in Europe [4].

In this scenario, conventional fuels such as gasoline and diesel are expected to be replaced by carbon-free renewable alternatives. The most attractive option is probably the switch to Battery Electric Vehicles (BEVs). However, the future availability of specific materials (such as lithium, cobalt, or nickel), the low energy density of current batteries, and the fact that their implementation does not strictly mean a reduction in GHG emissions – BEVs emissions are related to electricity production – make their application to the entire fleet of transport vehicles not optimal. In this sense, a massive BEV implementation may lead to an undesired rise in GHG emissions if non-renewable energy sources are used to feed the grid. In addition, the overall efficiency of the system could be reduced, increasing the energy demand and resulting in higher energy prices [5].

The use of current internal combustion engine (ICE) power plants still represents one of the most realistic options to achieve an efficient and effective decarbonization of transportation if combined intelligently with alternative fuels, electrification, and the use of renewable energy sources. A multitude of new fuel options are being evaluated, such as hydrotreated vegetable oil (HVO), synthetic hydrocarbon fuels made from biomass (BtL), dimethyl ether (DME), oxymethylene dimethyl ethers (OMEx), alcohols (ethanol, methanol, or butanol), among others [6]. All of them are interesting from the point of view of low GHG footprint considering both their production and use in energy generation.

The Environmental Protection Agency (EPA) believes that methane or its commercial surrogate, compressed natural gas (CNG), could be a viable fuel in the near future. The high hydrogen-carbon ratio (H/C) of CNG reduces CO_2 and particulate matter (PM) emissions during

* Corresponding author.
E-mail address: jogoso1@mot.upv.es (J. Gomez-Soriano).

https://doi.org/10.1016/j.enconman.2023.117259
Received 30 January 2023; Received in revised form 21 April 2023; Accepted 3 June 2023

combustion [7]. Moreover, the higher octane number of CNG compared to gasoline allows for the use of higher compression ratios, resulting in improved thermal efficiency. CNG can be obtained from renewable sources, such as anaerobic digestion (AD), where organic materials like food waste, sewage sludge, livestock waste, crop residues, or sequential crops are decomposed into biogas containing 50% to 70% of CH_4, with the remaining percentage being CO_2. Additionally, the organic waste used in this process can be utilized to generate bio-fertilizers, contributing to the development of a circular economy. Lee et al. [8] analyzed the environmental impacts of different anaerobic digestion technologies applied to sludge for energy production, and found that renewable CNG production could reduce GHG emissions by 39% in the worst-case scenario. Although the share of biogas is still small in most developed countries, it is expected to increase in the future [9]. When applied to road transport applications, CNG vehicles are considered a better option for passenger transport, both in urban and intercity settings, compared to diesel vehicles in terms of equivalent CO_2 emissions and total cost of ownership (TCO) [10].

Hydrogen (H_2) is a potential alternative to current fossil fuels. Recent studies have demonstrated the potential of hydrogen direct injection (H2-DI) in achieving high performance and efficiency. By controlling the timing of the intake valve closing and exhaust valve opening, researchers achieved an impressive 42.2% brake thermal efficiency (BTE) [11]. However, retrofitting conventional internal combustion engines with port fuel injection (PFI) is more straightforward and less expensive than converting them to direct injection. A review of the literature reveals that research on the conversion of existing gasoline engines to hydrogen internal combustion engine (HICE) prototypes is commonly found [12]. In addition, hydrogen PFI offers other advantages, including longer mixing time and optimized injection parameters.

Despite its excellent combustion properties, hydrogen-powered engines face similar disadvantages as BEVs. If water electrolysis is used to split water into hydrogen and oxygen (O_2), the bottleneck to achieving a complete CO_2-free energy production chain is electricity. Therefore, a largely GHG-free grid production is necessary to ensure a real GHG-free H_2 fuel (green hydrogen) with a low environmental footprint. Despite this huge challenge, hydrogen is expected to play a key role in future decarbonization plans in Europe. For example, in the European Union (EU), 40% of the total natural gas-based heating systems will be adapted to use 7% (in volume) of hydrogen-compressed natural gas (HCNG) fuel blends by 2030, and 32% HCNG by 2040 [13].

Due to the evident synergy between both fuels, several researchers have investigated the use of HCNG blends as an alternative fuel for internal combustion engines. Adding hydrogen to CNG has been shown to extend dilution limits and improve combustion stability [14]. Duan et al. [15] proposed an improved particle swarm algorithm optimized back propagation neural network method to study HCNG flame propagation. Du et al. [16] studied the effects of turbulent intensities and equivalence ratios on the flame structure of outwardly propagating HCNG-premixed flames. Kosmadakis [17] examined the cyclic variability in a spark-ignition (SI) engine fueled with CH_4/H_2 blends using a computational fluid dynamics (CFD) code. Mehra et al. [18] summarized the expected benefits of HCNG in terms of performance, emissions, and other relevant parameters in a review. Furthermore, Pandey et al. [19] found that smaller amounts of hydrogen in CNG could avoid costly and complex engine modifications required to achieve maximum brake torque ignition timing, making the conversion to HCNG a more viable option for vehicles [20]. Additionally, Gupta et al. [21] demonstrated the reduced environmental impact of HCNG-fueled vehicles throughout their life cycle, highlighting its potential as a promising alternative fuel. In a study conducted by Sagar et al. [22], the knocking characteristics of a single cylinder port fuel injected SI engine were examined using different fuels, including hydrogen and HCNG mixtures. The study found that hydrogen-enriched natural gas led to reduced emissions of CO_2, hydrocarbons (HC), and carbon monoxide (CO), but resulted in increased nitrogen oxides (NO_x) emissions.

The production of NO_x is a major concern associated with high-hydrogen content fuels. Numerous studies have been conducted to address this issue in HCNG-fueled engines. Park et al. [23] evaluated two dilution methods and found that the lowest engine-out NO_x emissions were observed under lean combustion. Similarly, Rao et al. [24] developed a quasi-dimensional combustion model with exhaust gas recirculation (EGR) [25] to predict NO_x emissions. Prasad et al. [26] investigated the combustion, performance, and emission characteristics of different HCNG mixtures under identical maximum brake torque timing using laser-induced ignition and spark ignition techniques. Laser ignition reduced the kernel flame formation and propagation time and produced less NO_x than conventional spark ignition [27].

The various investigations conducted so far highlight the complexity of achieving GHG-free mobility. Fuel production, costs, and availability, as well as vehicle manufacturing and operational requirements, are some of the key aspects that need to be considered for a progressive and realistic decarbonization of transportation. HCNG fuel blends may offer an intermediate and flexible solution to adapt propulsion requirements while optimizing the transition to a fully-developed hydrogen economy. In this sense, natural gas can partially meet the energy demand until green hydrogen becomes more widely available. Despite the large number of investigations, almost all of them focus on giving a very specific view of a particular situation which is difficult to extrapolate to other cases (i.e. focusing on a specific technology, operating strategy...). However, the current situation demands a more general vision that allows a quick adaptation to the changing conditions of the environment, such as the economy, socio-political interests and environmental factors.

The objective of this investigation is to evaluate the performance and emission levels of a single-cylinder spark-ignition (SI) engine fueled by HCNG blends, considering different scenarios based on the availability of green hydrogen. This method will help establish an optimized roadmap towards the use of hydrogen as a sustainable fuel for the future. As a result, the optimal share of hydrogen in the fuel blend to be targeted in further development steps (i.e. at a multi-cylinder or vehicle levels) can be defined based on the current situation in each region, significantly reducing the global warming footprint of transportation during the transition process. This strategy represents a significant step forward, as it not only focuses on the ultimate goal of a fully-developed hydrogen economy, but also allows for flexible adaptation during the transition. In this sense, the study brings together current technologies and strategies to be applied and re-adapted to the external factors, contributing to the current knowledge gap.

2. Materials and methods

This section presents a detailed description of the tools and methods employed in the investigation, with the aim of providing a clear and concise picture of the experimental techniques and procedures.

2.1. Experimental tools

The experimental campaign was carried out on a single-cylinder SI research engine equipped with a port fuel injection system. The main engine specifications listed in Table 1 were the same as those used in a previous investigations [28,29]. The fuel blend, which was injected using two different injectors, allowed enhanced control over the mixing and injection processes. Both injectors utilized in the study were Zavoli JET Injectors specifically designed for gaseous fuels. These devices are capable of operating at a maximum pressure of 4.5 bar and within a temperature range of −40 °C to 120 °C. The discharge nozzle of each injector has a diameter of 3 mm.

Fig. 1 depicts the schematic of the test cell used in this research. The original test bench layout was modified to accommodate dual gaseous

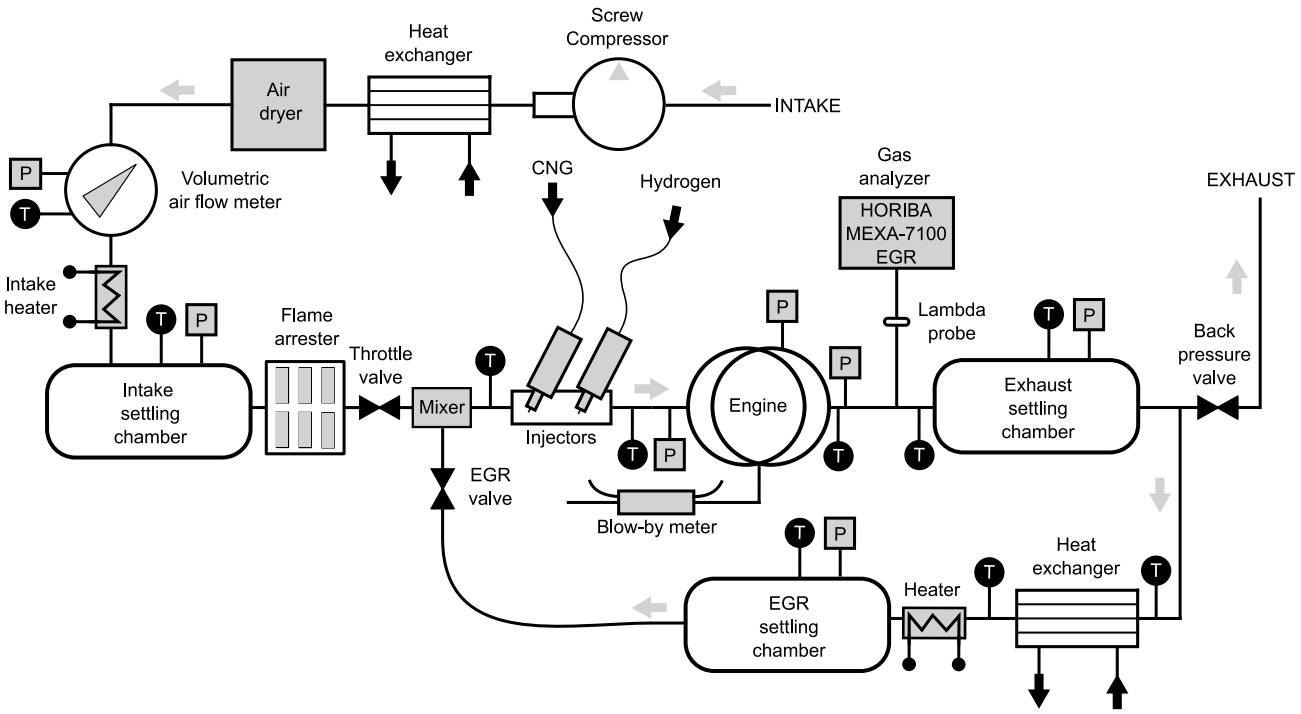

Fig. 1. Test bench layout.

Table 1
Engine specifications.

Number of cylinders	1
Displaced volume	454.2 cm^3
Stroke	86.0 mm
Injection systems	PFI
Ignition system	Spark plug
Cylinder diameter	82.0 mm
Compression ratio	10.7
Connecting rod length	144.0 mm
Valves per cylinder	2 intake, 2 exhaust
Engine management system	AVL PREMS GDI
Combustion system	4-valve pent roof GDI
IVO*	−380 CAD
IVC*	−135 CAD
EVO*	−600 CAD
EVC*	−338 CAD

*with respect to the firing TDC (0 CAD)

fuel strategies. In-cylinder pressure was measured using a piezoelectric sensor, while exhaust emissions were recorded using a HORIBA MEXA-7100EGR device. The mass flow rate of both fuels was controlled by two flowmeters: Bronkhorst F-113AC-1M0-AAD-55-V for hydrogen, and F-113AC-M50-AAD-55-V for CNG. The experimental facilities provided comprehensive control over all relevant parameters. Boost conditions were achieved using an external compressor, and the exhaust back pressure was regulated by a knife-gate valve located on the exhaust line. The accuracy of the instrumentation is presented in Table 2, and the precision of the gaseous pollutant measurements is shown in Table 3.

In terms of fuel definition, CNG was obtained directly from the Spanish natural gas network and compressed. Its composition consisted of 89.95% methane, 6.27% ethane, and other impurities. On the other hand, hydrogen was supplied in pressurized tanks. Further details about both fuels are summarized in Table 4.

Engine and combustion-related output parameters, such as Indicated Mean Effective Pressure (IMEP), cycle-to-cycle variability expressed by the IMEP covariance (COV_{IMEP}), emissions levels, and indicated efficiency, were computed using an in-house combustion diagnostics tool [30]. The tool was adapted for hydrogen, CNG, and HCNG fuel blends.

The referred combustion diagnosis tool estimates the energy released during combustion by resolving the energy equation with the measured in-cylinder pressure, and assuming several simplifications. For instance, it considers uniform pressure and temperature fields throughout the whole combustion chamber and several simplifications for estimating the heat transferred to the cylinder walls among others. It has been improved during some modifications [31] to reduce errors in the calculations.

The model originally considered three different components: air, fuel, and combustion products. The fuel component is now considered a single hydrocarbon ($C_xH_yO_z$) with equivalent properties of the real fuel mixture. The properties of this fuel element are weighted by the fuel composition used in each test as:

$$Y^{i}_{fuel} = \frac{\dot{m}^{i}_{fuel}}{\dot{m}^{1}_{fuel} + \dot{m}^{2}_{fuel}} \tag{1}$$

$$X^{i}_{fuel} = \frac{Y^{i}_{fuel}/M^{i}_{fuel}}{Y^{1}_{fuel}/M^{1}_{fuel} + (1 - Y^{1}_{fuel})/M^{2}_{fuel}} \tag{2}$$

Here, Y^{i}_{fuel} and X^{i}_{fuel} represent the fuel mass and molar fraction of each fuel element ($i \rightarrow \{CNG, H_2\}$), $\dot{m}^{i}_{fuel}$ is the mass flow rate and M^{i}_{fuel} the molar mass of $fuel^{i}$.

Therefore, the most relevant properties such as Lower Heating Value (LHV^{avg}), molar mass (M^{avg}) and density (ρ^{avg}) of the equivalent fuel can be computed as:

$$LHV^{avg} = LHV^{1}_{fuel} \cdot Y^{1}_{fuel} + LHV^{2}_{fuel} \cdot Y^{2}_{fuel} \tag{3}$$

$$M^{avg} = X^{1}_{fuel} \cdot M^{1}_{fuel} + X^{2}_{fuel} \cdot M^{2}_{fuel} \tag{4}$$

$$\rho^{avg} = Y^{1}_{fuel} \cdot \rho^{1}_{fuel} + Y^{2}_{fuel} \cdot \rho^{2}_{fuel} \tag{5}$$

Table 2
Instrumentation accuracy.

Signal (High frequency)	Sensor	Specification
In-cylinder pressure	Piezoelectric sensor	0 to 250 bar ± 0.3% linearity
Intake pressure	Piezoresistive sensor	0 to 10 ± 0.001 bar
Exhaust pressure	Piezoresistive sensor	0 to 10 ± 0.001 bar
Variable (Low frequency)	**Sensor**	**Specification**
Engine Speed	Optical angular encoder	1 to 6000 ± 1 rpm
Engine Torque	Strain-gauges torque-meter	−200 to 200 ± 1 N m
Intake pressure	Piezoresistive transducer	0 to 10 bar ± 1%
Exhaust pressure	Piezoresistive transducer	0 to 10 bar ± 0.3%
Intake temperature	Thermocouple type K	0 to 1000 ± 0.5 °C
Exhaust temperature	Thermocouple type K	0 to 1000 ± 0.5 °C
Fluid temperature	Pt100 thermoresistance	−200 to 850 ± 0.3 °C
Air mass flow	Air flow meter	0.6-100 m^3/h ± 1%
Hydrogen mass flow	Thermal mass flow meter	200–1600 l/min (based on N_2) ± 0.5%
CNG mass flow	Thermal mass flow meter	200–1600 l/min (based on N_2) ± 0.5%

Table 3
Accuracy levels of HORIBA MEXA 7100 DEGR for measurements of gaseous pollutants.

Pollutant	Analyzer	Range	Accuracy
HC	FID	min. 0 to 10 ppm C max. 0 to 50 kppm C	± 3%
NO_x	CLD	min. 0 to 10 ppm max. 0 to 10 kppm C	± 3%
CO	NDIR	min. 0 to 3 kppm C max. 0 to 12 vol%	± 3%
CO_2	NDIR	min. 0 to 5 kppm C max. 0 to 20 vol%	± 3%
O_2	PMA	min. 0 to 5 vol% max. 0 to 25 vol%	± 3%

Table 4
Specifications of CNG and H_2 fuels.

Properties	CNG	H_2
RON	120	> 130
AF_{st}	16.00	34.3
LHV	46.87 MJ/kg	119.9 MJ/kg
H/C	3.79	–
O/C	0.026	–
Molar mass	17.77 g/mol	2.01 g/mol
Purity	–	≥ 99.9%

$$Y_C^{avg} = Y_{fuel}^1 \cdot Y_C^1 + Y_{fuel}^2 \cdot Y_C^2 \quad (6)$$

$$Y_H^{avg} = Y_{fuel}^1 \cdot Y_H^1 + Y_{fuel}^2 \cdot Y_H^2 \quad (7)$$

$$Y_O^{avg} = Y_{fuel}^1 \cdot Y_O^1 + Y_{fuel}^2 \cdot Y_O^2 \quad (8)$$

2.2. Definition of scenarios

This section describes the basis of the method used to simulate the transition to a fully-developed hydrogen economy, considering different scenarios based on the availability of green hydrogen. The assessment of the complete decarbonization of the transport sector, particularly from a tank-to-wheel perspective, is conducted through four different situations that progress from the use of a current fossil fuel (CNG) to the ultimate scenario of using H_2 as fuel. Accordingly, it should be possible to define the optimal fuel composition that ensures a substantial reduction in GHG emissions. Fig. 2 provides a summary of the key aspects of each scenario, including the transition from CNG (Step I), low hydrogen substitution (Step II), high hydrogen substitution (Step III), and finally hydrogen (Step IV).

In the current situation (Step I), where there is limited infrastructure for green hydrogen production, CNG could serve as an alternative to conventional fuels. With anticipated advancements in biogas production and improvements in CNG-powered engines, it may be possible to achieve a reduction in GHG emissions without changing the fuel composition. This initial scenario is thus centered on enhancing the CNG combustion process, reducing NO_x emissions, and minimizing thermal losses through the implementation of a dilution strategy.

Disadvantages of lean combustion, such as high cycle-to-cycle dispersion that limits engine performance, will be attempted to be overcome in the second scenario (Step II). In this scenario, a small amount of H_2 will be required to improve CNG combustion features. Combining Steam Methane Reforming (SMR) with Carbon Capture and Storage (CCS) techniques could help introduce enough hydrogen to control CNG combustion instabilities at the beginning of the transition process. Additionally, these quantities of hydrogen can be obtained through an onboard reforming system [32]. In this way, the hydrogen line can be removed from the vehicle, avoiding the need for large amounts of H_2 storage and subsequently minimizing the range distance penalties associated with low hydrogen density. This approach can be initially implemented in niche fleets and later extended to other vehicle types as local hydrogen grids are established.

As the distribution, production, and storage challenges associated with H_2 are solved, green hydrogen will reduce energy costs, boost industrial competitiveness, and also diversify energy sources. In this scenario (Step III), an extensive refueling station network and pipeline infrastructure will be built. The focus is no longer on improving CNG combustion, but rather on reducing the carbon content of the fuel. Additionally, a wider dilution range can be achieved thanks to hydrogen combustion properties, which is expected to result in efficiency gains.

In the final scenario (Step IV), only hydrogen is used as a fuel for ICEs. This scenario represents a fully-developed hydrogen economy where fossil fuels are completely replaced. Decoupling the demand for resources from access to highly efficient energy production can help achieve zero effective emissions. Similar to the previous scenario, the objective is to identify the optimal dilution conditions for achieving the lowest fuel consumption.

2.3. Definition of operating conditions

An experimental campaign was conducted to compare the engine performance and emission levels (including pollutants and greenhouse gases) under the scenarios defined above. The engine operating conditions used for each scenario are summarized in Table 5.

As it can be seen, two engine speeds (1500 and 3000 rpm) and three engine loads (4, 7 and 10 bar of IMEP) are studied, being enough representative of real driving conditions. The operating conditions are referred by a pair of numbers ([rpm]@[bar]) representing the engine speed and engine load (IMEP). The IMEP targets were established by operating the engine with a stoichiometric CNG mixture without the use of external EGR. Once the desired load level was achieved,

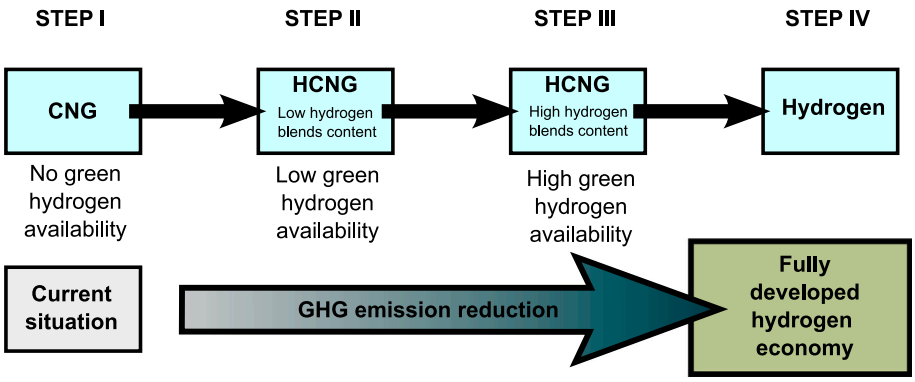

Fig. 2. Diagram of the proposed method based on the different scenarios to mimic the fuel transition.

Table 5
Test matrix definition.

Operating point	Step I	Step II	Step III	Step IV
1500@4	$\lambda = [1, \lambda_{max}^{CNG}]$	λ_{max}^{CNG}	–	λ sweep
1500@7	$\lambda = [1, \lambda_{max}^{CNG}]$, EGR_{max}^{CNG}	λ_{max}^{CNG}	λ sweep	λ sweep
1500@10	$\lambda = [1, \lambda_{max}^{CNG}]$	λ_{max}^{CNG}	–	–
3000@10	$\lambda = [1, \lambda_{max}^{CNG}]$	λ_{max}^{CNG}	–	–

the fuel energy was calculated based on the injected mass of CNG and its LHV. Subsequently, the injected fuel mass was adjusted to maintain the same energy available for combustion at that particular load level. As a result, the amount of injected fuel mass is reduced as the hydrogen percentage is increased in the fuel blend due to its higher LHV. Specifically, for an equivalent CNG condition, the amount of H_2 is 60% lower. Furthermore, it should be noted that under these conditions, the IMEP level may vary if the thermal efficiency changes due to modifications in other parameters, such as the dilution ratio or combustion phasing. Therefore, the target values of engine load, which are used to designate the operating points, should be viewed as qualitative references that simply indicate whether the engine load is low, medium, or high.

In most research works, the hydrogen content in the fuel blend is expressed in volumetric fraction. However, the authors chose the mass fraction as the characterization parameter because it facilitates discussion in the scenarios considered. Fig. 3 illustrates the equivalences between different ways of characterizing mixtures in terms of hydrogen content.

The energy deposition provided by the spark plug was maintained in all tests. The intake temperature measured at the surge tank was fixed at 308.15 K, and oil and coolant temperatures were kept constant at 363.15 K. The dilution ratio (air-to-fuel ratio) was controlled through the intake pressure. Three repetitions of each test were recorded to reduce the uncertainty of the measurements. The results presented in the following sections correspond to the average value of these three repetitions.

Depending on the scenario considered, some aspects of the methodology have been adapted according to:

- In Step I, four operation conditions (1500@4, 1500@7, 1500@10, and 3000@10) were studied. The spark timing (ST) was case-by-case optimized to reach the maximum brake torque (MBT) limit at stoichiometric and maximum-diluted conditions. The latter situation is achieved when 5% of COV_{IMEP} is exceeded. Also, the impact of diluent composition – air–fuel ratio (λ) vs. exhaust gas recirculation – was analyzed through an ST sweep comparison.
- In the second scenario (Step II) low hydrogen content fuels with 1% of H_2 by mass (HCNG1), 2% (HCNG2), and 3% (HCNG3) were analyzed. This upper limit was fixed to avoid high volumetric losses and abnormal combustion phenomena such as pre-ignition or backfire. The same operation conditions used for Step I were considered in the analysis. The air-to-fuel ratio was obtained also from the previous scenario, being stabilized by the maximum dilution achieved in each operating condition.
- The third scenario (Step III) focuses on evaluating high hydrogen content fuels. Since the amount of H_2 in the fuel blend increased significantly, the effect of higher dilution was also studied. Sweeps of λ were measured at the MBT limit from close stoichiometric ($\lambda \approx 1.2$) to ultra-lean conditions ($\lambda > 2$). The analysis was focused only on the operating condition 1500@7. The fuel composition was defined by increasing the hydrogen amount in 25% steps (HCNG25, HCNG50, and HCNG75).
- Finally, hydrogen combustion was assessed at two operation conditions (1500@4 and 1500@7) in Step IV. The idea is to give an overview of the main limitations when operating a PFI SI engine with hydrogen fuel. The analysis was focused on the same boundary conditions considered for the previous scenario.

3. Results

Results are divided into four sections, analyzing in detail the performance and emission levels under each of the proposed scenarios.

3.1. No hydrogen fuel availability

The target of this first study is to establish an initial reference for future comparisons, giving an overview of a situation similar to the current one. First, Fig. 4 shows a comparison of diluent compositions under the operating condition 1500@7. In general, the stable ST window is reduced with respect to the stoichiometric case when considering any type of dilution. This is particularly evident in the case of air dilution ($\lambda_{max} = 1.47$) where the stable ST window is reduced from 14 to 12 CAD. In addition, this window is systematically advanced, moving the MBT point from −14 CAD aTDC to −26 CAD aTDC for the air dilution case, and to −34 CAD aTDC for the EGR dilution case ($EGR_{max} = 21\%$).

The MBT case for λ_{max} conditions reports approximately 15% more IMEP than the stoichiometric case ($\lambda = 1$). This gain decreases up to 3% when considering EGR dilution. Trends of Gross Indicated Efficiency (GIE) are analogous to the IMEP profiles. As expected, the highest values of GIE are achieved for the air dilution cases, reaching almost 37%. Using EGR dilution is possible to achieve slightly higher levels compared with the non-diluted case (35% from 33%). Cycle-to-cycle variation (CCV) is analyzed through COV_{IMEP} parameter. Results show how combustion stability is strongly compromised when delaying the ST in diluted conditions. While the non-dilution tests are able to burn properly even at delayed ST (around −10 CAD aTDC), dilution tests experience a significant combustion instability at a given ST. This point is around −22 CAD aTDC for the air dilution and around −28 CAD aTDC

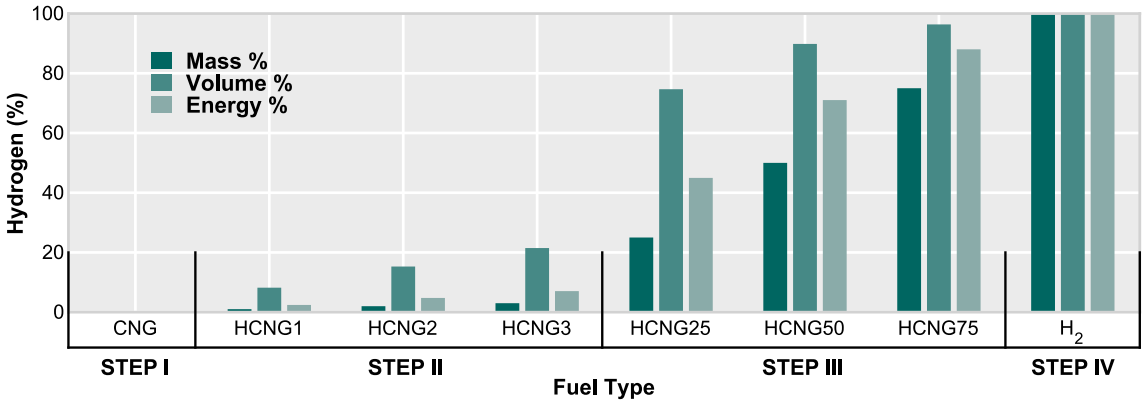

Fig. 3. Characterization of fuel blends as a function of hydrogen percentage on mass, volume, and energy content.

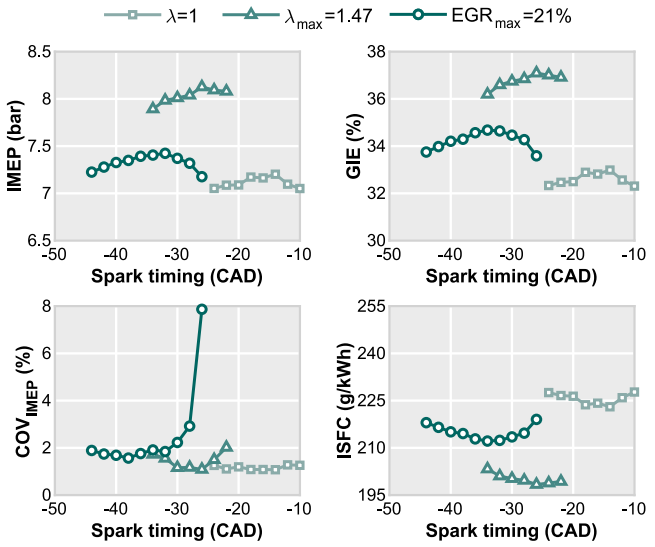

Fig. 4. Performance levels comparison. Different dilution strategies (no dilution, air and EGR) are considered at 1500 rpm and 7 bar of IMEP.

for the EGR dilution. Regarding fuel consumption, dilution strategies reduce ISFC achieving an optimal point of 198 g/kWh at maximum air dilution conditions.

Trends of main pollutant and GHG emissions are plotted in Fig. 5. Since methane has 25 times more greenhouse effect than CO_2, unburned HC should be considered in the GHG analysis. In this investigation, it was not possible to discretize the HC measurement into methane and other intermediate species. However, the chemical characteristics of methane (dissociation energy, chain length, etc.) make the amount of HC intermediate species at the exhaust tailpipe negligible. Therefore, the unburned HC measurement included in Fig. 5 can be qualitative, and to some extent quantitative, indicator of CH_4 emissions. In this case, unburned HC increased respect to non-diluted cases when using air dilution, especially at delayed ST. Similarly, HC emissions due to EGR dilution also increase at delayed ST.

Regarding pollutant emissions, NO_x are drastically reduced when diluting by EGR. Contrarily, air dilution shows comparable values to those of the non-diluted stoichiometric case, being higher for cases with larger ignition advance. The effect of the spark timing is higher for air-diluted conditions than for the non-diluted case. EGR dilution is less sensitive to ignition timing. CO emissions are comparable between the non-diluted and EGR-diluted cases, whereas they are significantly reduced in the case of air-dilution since the higher oxygen availability promotes CO oxidation to CO_2.

In view of the better results obtained with air dilution, the extension of the analysis to all operating points is carried out only considering this type of dilution. The study, presented in Figs. 6 and 7, is focused on the MBT case of the non-diluted stoichiometric and maximum λ tests at each operating point. A general improvement is observed in GIE and therefore in IMEP levels. This significantly improves the fuel consumption in all operating points, while maintaining combustion stability.

As far as emissions are concerned, due to the fact that part of the fuel is not completely oxidized in stoichiometric conditions, a NO_x emission increase due to a higher temperature and improved combustion performance at maximum λ is observed. Note that although HC levels are maintained, the amount of CO is drastically reduced.

3.2. Low hydrogen content in the fuel

This scenario was deeply analyzed by the authors in a previous publication [28]. Focusing almost exclusively on the combustion process analysis, the authors show the effect of small hydrogen substitution percentages. Results showed that combustion was enhanced by increasing the percentage of hydrogen in the fuel. The high flame speed and wide ignition limits of hydrogen accelerate the combustion process, improving combustion stability at high dilution conditions [33]. The HRR is systematically advanced to the compression stroke and significantly shortened under equivalent conditions. This causes an increment in the maximum in-cylinder pressure peak: around 10 bar when comparing the CNG and HCNG with 3% hydrogen concepts in the 3000@10 test. This faster combustion leads to a CCV reduction, and it also widens the stable operating range determined by the spark timing.

To see the impact of these effects on engine performance and emissions, the analysis performed is complemented by the results in Figs. 8 and 9. Here, the performance levels, emissions and other relevant parameter es are plotted for the four operating points considered so far at the MBT limit. Fig. 8 shows an optimum point around 2% of hydrogen substitution. IMEP and GIE parameters evince the highest values at this hydrogen content in all operating points. As revealed in [28], combustion stability is improved especially at low load (1500@4) and high load-speed (3000@10). Requirements of the boosting system can be estimated through the intake pressure inspection. This is especially relevant in the case of HCNG fuel blends due to the low density of hydrogen that may compromise the volumetric efficiency in a PFI system. Results do not show a critical rise in intake pressure due to the small amounts of H_2 present in the fuel, suggesting that volumetric losses are not relevant.

Regarding GHG emissions, Fig. 9 show an improvement in terms of both CO_2 and CH_4 (quantified through the unburned HCs) as the hydrogen content increase. This enhancement is a consequence of better GIE and combustion stability. NO_x emissions are not significantly

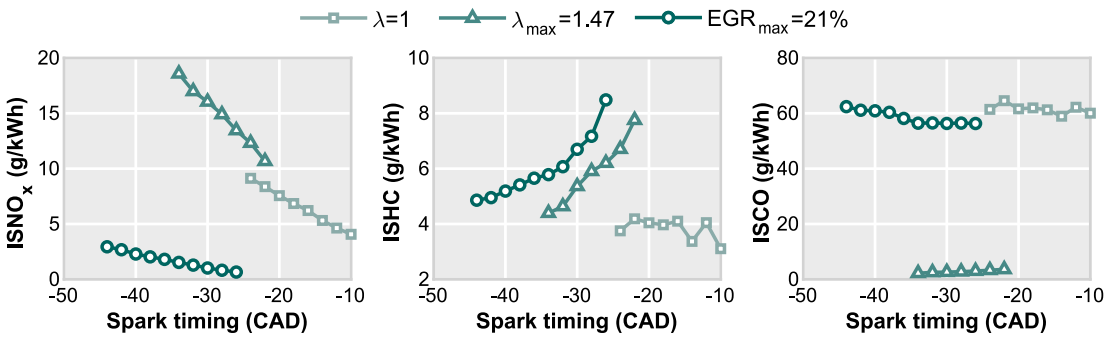

Fig. 5. Emission levels comparison. Different dilution strategies (no dilution, air, and EGR) are considered at 1500 rpm and 7 bar of IMEP.

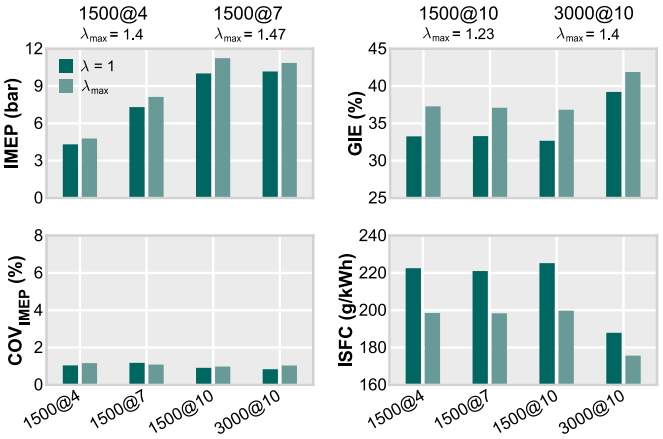

Fig. 6. Performance levels comparison at the MBT limit of all operating points.

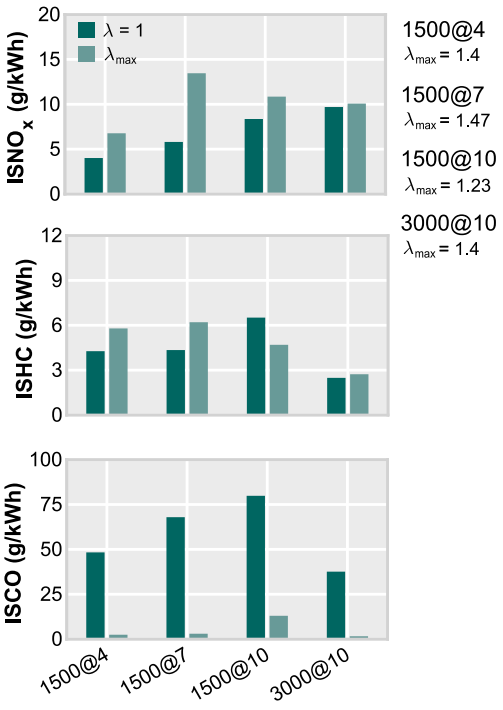

Fig. 7. Emission levels comparison at the MBT limit of all operating points.

affected by the increase of the H_2 percentage. As Fig. 9 shows, there is no clear relationship between hydrogen content and these emissions. The only substantial difference is that in general, HCNG cases have

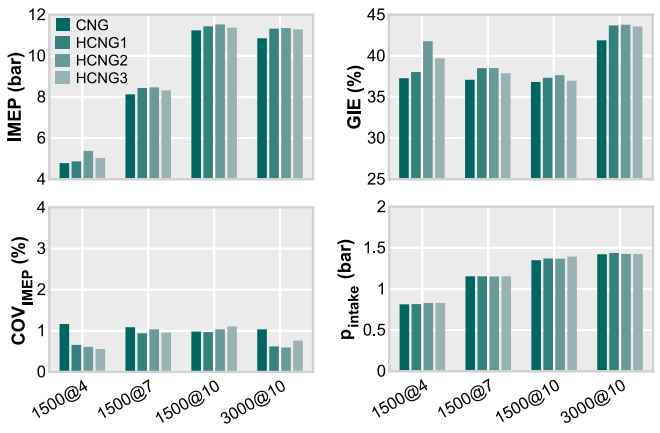

Fig. 8. Performance levels comparison. Different fuel compositions (CNG, HCNG1, HCNG2, and HCNG3) are considered at the MBT limit of 1500@4, 1500@7, 1500@10, and 3000@10.

slightly higher values than CNG cases, probably due to the higher local temperatures achieved due to H_2 addition. CO emissions depend on the operating point studied. Hydrogen helps to slightly reduce CO in the products at 1500@4, 1500@7 and 3000@10, whereas trends are not so clear at 1500@10.

In summary, low hydrogen substitution results in better performance outputs when small amounts of H_2 are considered. Higher combustion stability leads to enhanced control over combustion which extends the operating range. The higher thermal efficiency, the carbon substitution by hydrogen, and enhanced combustion stability help to reduce GHG emissions. CO emissions remain at the same level of CNG combustion while NO_x levels highlight the need for catalytic converters to deal with pollutant regulations.

3.3. High hydrogen content in the fuel

In this scenario, the operating point 1500@7 was chosen as the representative condition to continue with the investigation. Results of increasing hydrogen share to 25, 50, and 75% (in mass) are analyzed at different λ conditions.

Fig. 10 shows the performance level of each fuel composition and dilution condition. Again, IMEP and GIE values follow an equivalent behavior due to the testing method used in this investigation (same fuel energy per test). Therefore, the engine performance output is directly related to efficiency. There are two regions characterized by how λ affects these parameters. From stoichiometric conditions to $\lambda = 2$, each 0.2 λ increment grows efficiency by approximately 1%. Then, the efficiency-performance growth ratio is reduced for higher dilution rates. In this study, the maximum measured λ was determined by the

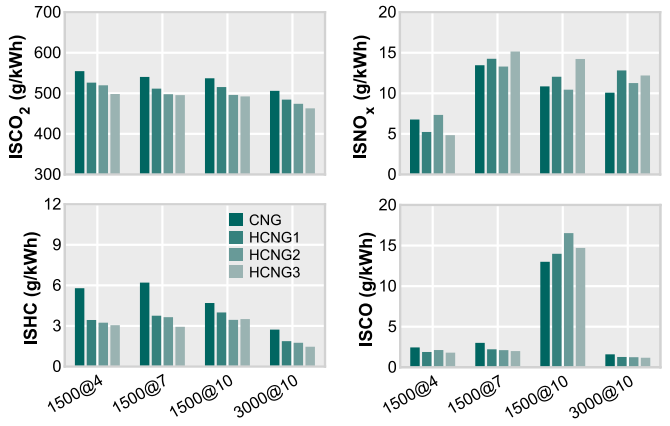

Fig. 9. Emission levels comparison. Different fuel compositions (CNG, HCNG1, HCNG2, and HCNG3) are considered at the MBT limit of 1500@4, 1500@7, 1500@10, and 3000@10.

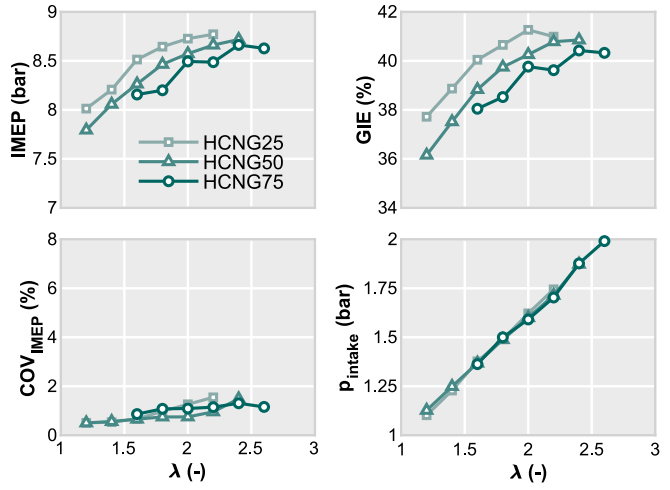

Fig. 10. Performance levels comparison. Different fuel compositions (HCNG25, HCNG50, and HCNG75) are considered at 1500 rpm and 7 bar of IMEP.

drop in efficiency, never reaching the point where the COV_{IMEP} exceeds 5%. Thus, the CCV remains bounded at all measured points, even at the highest diluted points.

Focusing on the effect of fuel composition, HCNG25 results show the highest values of GIE at the same λ above HCNG50 and HCNG75. As the hydrogen content increases the IMEP and GIE levels decrease whereas the maximum value is reached at a higher dilution ratio. This peak value is achieved at $\lambda = 2$ for HCNG25, $\lambda = 2.2$ for HCNG50 and $\lambda = 2.4$ for HCNG75. Since the combustion stability is not excessively altered in any of the conditions measured, the efficiency drop observed due to the hydrogen increase in the fuel should be directly related to the wall heat transfer. The high burning rate of hydrogen incites heat transfer losses by increasing convection while reducing the quenching distance. Shudo et al. [34] investigated the cooling losses in SI engines using CNG and H_2, showing higher cooling losses for hydrogen. Nieminen [35] studied the potential of hydrogen compared to gasoline as a fuel for ICE at the same air dilution. They demonstrated that hydrogen reduces heat rejection and blowdown during the exhaust stroke. In another work by Nieminen et al. [36] an exergy analysis pointed out that a HICE improves thermodynamic efficiency and reduces combustion irreversibilities. Nevertheless, less indicated work was obtained in comparison with gasoline because of the high thermal losses. Demuynck et al. [37] presented instantaneous heat flux measurements in a SI engine fueled with hydrogen and other relevant fuels. Results also indicated the negative effect of higher heat losses on engine efficiency. As a consequence, to maintain a high engine efficiency high dilution strategies (air dilution and/or EGR) should be applied to HICE port fuel injection engines.

Examination of intake pressure values reveals a direct relationship with the target dilution ratio. Moreover, there is no significant effect due to the fuel composition since all lines practically overlap. This makes sense if considering that volumetric percentages of hydrogen are between 75% (HCNG25), and 95% (HCNG75).

The combustion stability is remarkable even at the leanest conditions where flammability is typically considered unstable for conventional fuels. It should be noted that the hydrogen concentration is notably high, with levels above 25% by mass and 75% by volume, resulting in flammability limits that are closer to those of hydrogen rather than CNG. Most of the studies referenced in the bibliography focus on lower hydrogen content within the ranges considered in our investigation. Nevertheless, Ma and Wang [38] reported stable combustion levels at a lambda value of 2.1 when using a 50% H_2 content (by volume) in a HCNG blend. Therefore, reaching a maximum lambda value of 2.2 when using HCNG25 with a 75% hydrogen volume content seems reasonable to conclude that the values obtained are realistic.

To better understand these trends, Fig. 11 shows the in-cylinder pressure and the HRR profile for thee hydrogen content levels (HCNG25, HCNG50, and HCNG75) when operating at 1500@7 λ = 2 MBT conditions. An examination of these signals reveals that an increase in H_2 substitution has a pronounced effect on HRR, leading to sharper profiles and higher peak values. Furthermore, the cycle-to-cycle variability, as indicated by the shadow area, decreases to a certain extent with increasing hydrogen substitution.

The effect of air dilution on the combustion process is illustrated in Fig. 12. As evident from the figure, hydrogen accelerates combustion, resulting in a shorter combustion duration. Specifically, when switching from 25% to 75% of H_2 substitution, the CA90-10 is reduced by approximately 10 CAD. Consequently, the ST must be advanced to maintain the optimum combustion phasing (CA50). Furthermore, the maximum peak of heat release rate (HRR) also increases with the hydrogen content. These trends are consistent across all λ values considered in this study.

As in the previous sections, the emission levels measured for the three fuel blends are plotted in Fig. 13. Focusing on specific CO_2 emission values ($ISCO_2$), it is evident how they are related to the fuel composition. Obviously, the more H_2 in the fuel, the less CO_2 produced by combustion. In this way, HCNG25 made approximately 300 g/kWh of $ISCO_2$ whereas HCNG50 and HCNG75 reduced this level up to 170 g/kWh and 70 g/kWh, respectively. Increasing the degree of dilution λ slightly reduces $ISCO_2$ emission due to thermal efficiency gains observed in Fig. 10. However, the effect of dilution is not comparable to that of fuel composition. Emissions of unburned HC (mostly CH_4) and CO follow a similar trend. They are notably reduced as the amount of hydrogen is increased in the fuel blend and the number of carbon atoms is progressively reduced. Because of this, the effect of λ is also different as the fuel shifts towards less carbon content. While unburned HC increase by almost 0.5 g/kWh with 25% of H_2 content (from $\lambda = 1.2$ to $\lambda = 2.2$), in the case of 75% this increase is around 0.01 g/kWh (from λ = 1.6 to λ = 2.6). Similarly, CO emissions rise from 1 to 1.6 with HCNG25 whereas they roughly remain constant around 0.35 g/kWh. NO_x emissions show a completely different pattern. The reduction is a consequence of the dilution increasing rather than the fuel composition. Data evince an inflection point between $\lambda = 1.5$ and $\lambda = 2$. In this range, NO_x emissions are reduced from 20 g/kWh to nearly zero levels for all assumed fuels. It seems the maximum local temperatures as a result of combustion do not change excessively with fuel composition. This is to some extent to be expected since both fuel components have similar adiabatic flame temperatures: $T^{ad}_{CH_4}$ = 2226 K vs. $T^{ad}_{H_2}$ = 2254 K (for stoichiometric combustion with standard air).

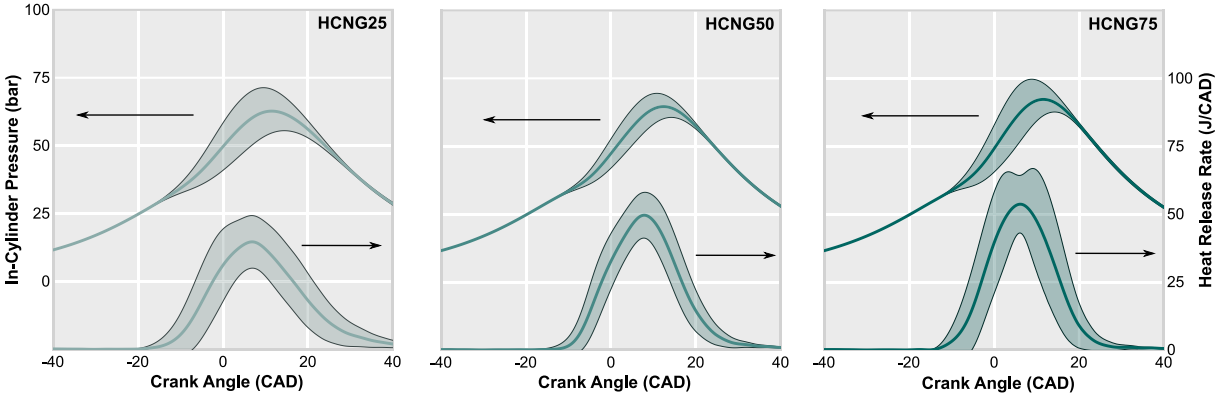

Fig. 11. In-cylinder pressure and HRR profiles for different fuel compositions (HCNG25, HCNG50, and HCNG75) operating at 1500@7 λ = 2 MBT conditions.

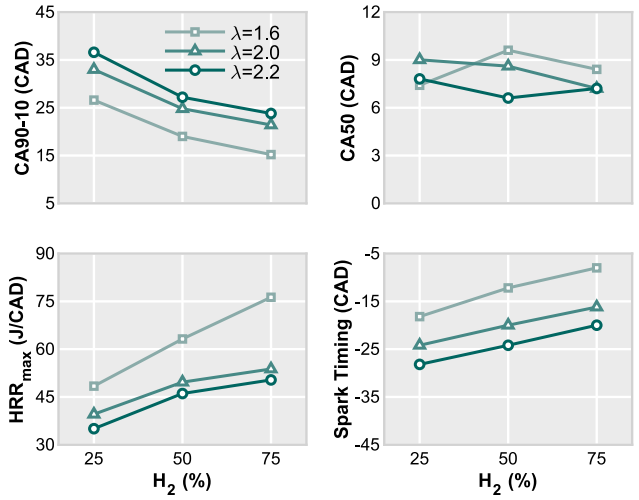

Fig. 12. Combustion parameters for different fuel compositions (HCNG25, HCNG50, and HCNG75) and dilution ratios operating at 1500@7 MBT conditions.

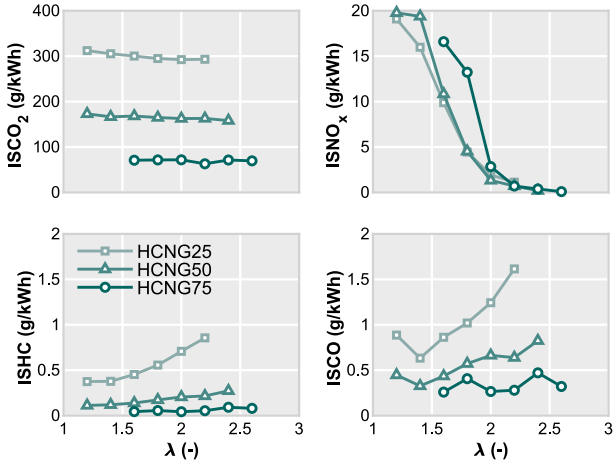

Fig. 13. Emission levels comparison. Different fuel compositions (HCNG25, HCNG50, and HCNG75) are considered at 1500 rpm and 7 bar of IMEP.

In summary, the application of these high-content H_2 fuels to transportation could be inferred a strong reduction on CO_2 emissions as the hydrogen percentage is increased. Moreover, the use of catalytic converters for NO_x control could be avoided with the operation with the correct dilution ratio.

3.4. Hydrogen fuel

This section analyzes the application of hydrogen as fuel, considering two representative conditions: 1500 rpm with 4 and 7 bar of IMEP. A air dilution sweep was performed under both operating conditions. The limits of the sweeps were conditioned by combustion abnormalities due to knock and maximum thermal efficiency. These values range from 1.4 to 4 for the low-load case and, 2.4 to 3.4 for the high-load case.

Results of the main performance outputs are presented in Fig. 14. In both operating points, the maximum efficiency and performance values are found around λ = 3. Increasing air dilution from this point on deteriorates the engine performance due to CCV. In these leaner conditions, combustion instabilities result in higher losses than gains in efficiency. The main difference between the two operating points lies in the effective dilution range. While at low load (1500@4) there is almost no knock limitation and combustion stability over a wide λ range (1.4–4), this range is much narrower as the load increases (2.4–3.4). This results in a reduced range of efficiency variation: ~4% to ~1%.

Only unburned hydrogen, NO_x and water are the awaited HICE exhaust gasses. No carbon dioxide or carbon monoxide are expected to be emitted due to H_2 combustion. However, small amounts of these elements were recorded during the experimental campaign as a consequence of the interaction of H_2 with the lubricant [39]. Fig. 15 will focus on the analysis of nitrogen oxides as the main pollutant of HICE.

At low load conditions, the maximum NO_x emission values are recorded at λ = 1.4, being the lower dilution conditions tested. Increasing air dilution reduces combustion temperatures, inhibiting the thermal NO_x formation mechanism, leading to considerably low values for λ around 2 (< 1 g/kWh).

4. Discussion

Results of previous section demonstrate the potential of hydrogen as a carbon-neutral fuel if its production is based on renewable energy sources. However, they have also shown that the way in which society transition to this scenario can have a significant effect on CHG and pollutant emission levels. The objective of this section is to provide a set of guidelines to help identify the best operating strategy for HCNG-ICEs based on the availability of green hydrogen.

The operation point 1500@7 was selected to be the reference due to the wide range of conditions measured. Fig. 16 summarizes the emission levels registered considering all the situations studied throughout the four scenarios.

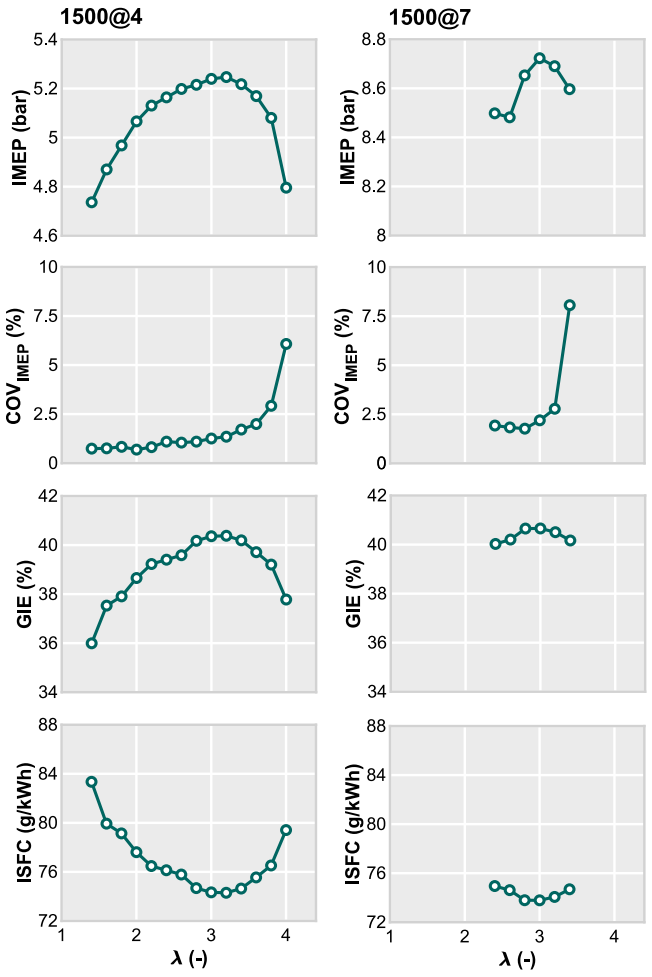

Fig. 14. Performance and efficiency results for H_2 combustion considering two operating points.

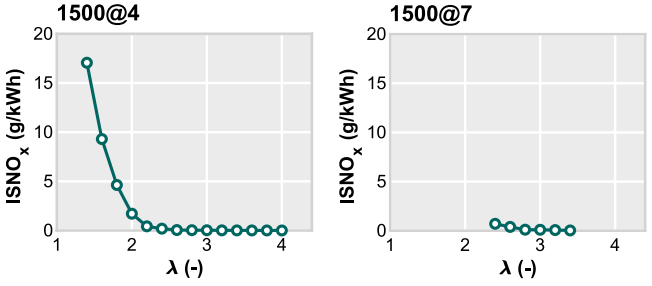

Fig. 15. NO_x emission levels registered for H_2 combustion considering two operating points.

Inspection of $ISCO_2$ reveals the relationship between the amount of H_2 in the fuel and the CO_2 reduction. However, the gain in thermal efficiency also results in CO_2 reduction without the need for carbon-based fuel substitution. Results of the second scenario (Step II), in which small amounts of hydrogen were studied, evince a significant reduction compared to the CNG case (see left in-zoom view of Fig. 16). In this situation, the mechanism responsible for the improvement in CO_2 emissions is not evident, since the percentage of substitution is small and the gain in efficiency is considerable. In contrast, the improvement in thermal efficiency as dilution increases for larger amounts of H_2 (Step III) does not seem to have an impact comparable to that produced by H_2 substitution. These effects can be better appreciated in Fig. 17,

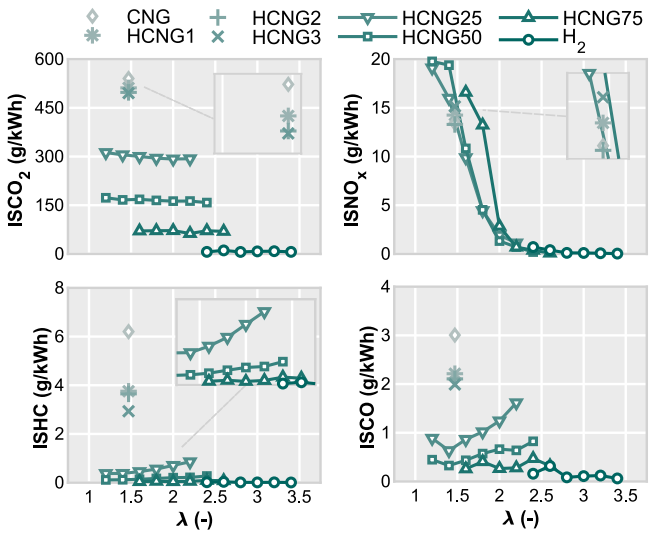

Fig. 16. Summary of exhaust emissions for the operation point 1500@7 considering all fuel compositions.

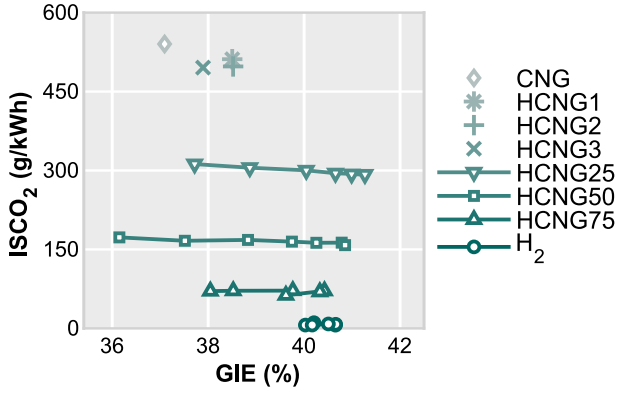

Fig. 17. $ISCO_2$ vs. GIE for the operation point 1500@7 considering all fuel compositions.

where the specific CO_2 emissions are drawn against the GIE. From Step I to Step II, the indicated efficiency increases almost 1.5%, lessen the CO_2 by 45 g/kWh. In Step III, these increments of GIE are notably higher (2.5%–5%) but with lower CO_2 reductions (15–20 g/kWh).

The results from Step IV reveal non-zero emissions of CO_2 and CO even considering the fact that the fuel is carbon free. Previous research works [40] have indicated that CO and CO_2 can be present in the exhaust gases of SI engines fueled with pure hydrogen. These carbon-bearing species are formed due to the oxidation of lubricating oil and can serve as natural tracers for indicating oil consumption through combustion. Hydrogen, with its small quenching distance, has the ability to extend combustion into narrow gaps and crevices, potentially leading to higher consumption of lubricating oil compared to conventional fuels. However, it remains uncertain to what extent the presence of hydrogen in the cylinder mixture chemically contributes to the observed oil consumption. The temperature of the engine surface and the bulk temperature of burnt products are strongly influenced by thermal loading, which is a contributing factor to increased rates of oil consumption.

A numerical study was performed in order to shed some light on the influence of these two parameters on CO_2 removal. This study uses an energy balance to convert the amount of fuel used into specific CO_2 emissions, allowing both effects (H_2 substitution and thermal efficiency gain) to be decoupled when considering a single-step complete combustion. Results are presented in Fig. 18, showing a CO_2 reduction map as

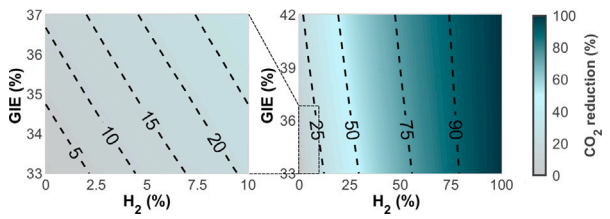

Fig. 18. CO_2 reduction map considering hydrogen percentage content and indicated efficiency.

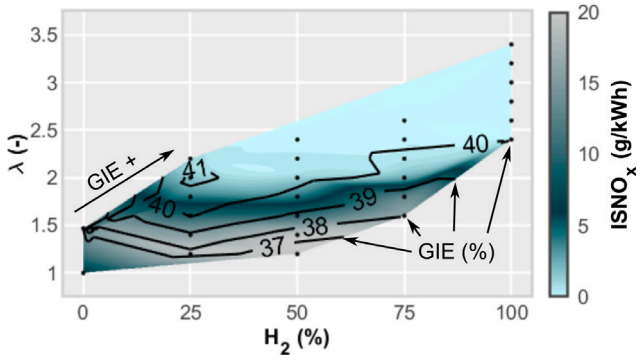

Fig. 19. NO_x emissions for the operation point 1500@7 considering all fuel compositions.

a function of the hydrogen content in the fuel and thermal efficiency variables. An increase of 2.5% of hydrogen causes a 5% reduction in CO_2, which is comparable to the reduction achieved by 2% of thermal efficiency gain. Both numbers being in range with the first and second scenario. With higher increments of hydrogen, the reduction in CO_2 emissions is remarkably larger than any reasonable gain in thermal efficiency. For example, for a mixture of 12% H_2, the CO_2 reduction is comparable to a 10% gain in thermal efficiency. Therefore, the performance improvement of HCNG-ICEs is more relevant in the first scenarios (Step I and II) where the amount of hydrogen is small. This relevance is diluted as hydrogen from renewable sources increases its presence, as it becomes a mere economic aspect due to the higher or lower fuel consumption.

Regarding NO_x emissions, it can be observed from Fig. 16 that it is a problem directly related to the dilution ratio. In this sense, the natural transition to a high hydrogen content is going in the right direction due to the properties of hydrogen, since it allows operating at sufficiently high air-to-fuel ratios to minimize this type of emissions. The issues with NO_x are expected in the early stages of this transition (Step II), where the low-hydrogen content in the fuel hinders the combustion stability at high dilution rates. This trend is clearly observed in Fig. 19. Here, the specific NO_x emissions are plotted against the percentage of hydrogen in the fuel and the λ. The highest levels of NO_x agglutinate at low λ whereas the lowest values correspond to the highest GIE levels. In terms of maximum performance, it is possible to distinguish an optimum region with values above 41% for fuel blends with 25% of H_2.

Finally, recalling the unburned HC and CO trends depicted in Fig. 16, a substantial reduction in ISHC (Indicated specific HC) as hydrogen percentage increases is observed. The two reasons for this reduction are the improvement in combustion efficiency and the reduction of carbon in the fuel composition. Including small hydrogen amounts allows reducing these emissions significantly in Step II. Nevertheless, the highest reduction occurs when a higher content of hydrogen is used in Step III. CO emissions have the same effect as for unburned hydrocarbons; the carbon reduction in the fuel composition and the improvement in combustion stability reduce them. However, the sensitivity to dilution is higher.

5. Conclusions

This paper proposes a new approach to mitigating the problem of greenhouse gas emissions. The investigation focuses on analyzing the effects of different scenarios with varying fuel compositions and dilution conditions on emissions and efficiency levels, aiming to establish the first step towards a flexible roadmap for a hydrogen-based economy. These scenarios are based on the availability of green hydrogen, which is crucial for achieving GHG emission-free transport. To this end, an extensive experimental campaign was conducted in a single-cylinder spark-ignition engine powered by HCNG blends at several representative operating points.

Experiments with low hydrogen content revealed that adding small amounts of hydrogen to the fuel (1%–3% by mass) helps stabilize combustion at moderate dilution ratios (λ = 1.4), resulting in an improvement in thermal efficiency by approximately 1.5%, and a reduction in CO_2 and CH_4 emissions.

The use of larger quantities of hydrogen (25%–75% by mass) results in a significant reduction in both GHG and pollutant emissions (HC and CO), leading to very low levels. However, thermal efficiency is conditioned as the percentage of H_2 increases, with increased heat transfer to the chamber walls being a key parameter that controls this trend. There is an optimum point that offers the best performance based on a specific quantity of hydrogen (25%) and dilution condition (λ = 2).

Further studies reveal that the loss of thermal efficiency as hydrogen increases in the fuel is compensated by the percentage of substitution of carbon elements, making it practically the only factor controlling CO_2 emissions for fuel blends with a H_2 content higher than 5% (by mass).

In the case of pure hydrogen combustion, where GHG emissions are not a relevant issue if fuel production is based on renewable sources, the problem seems simpler, at least initially. The solution is to find an engine platform that allows for operation with a reasonable thermal efficiency and minimizes NO_x generation as much as possible. In these conditions, small amounts of CO and CO_2 are measured due to the oxidation of lubricating oil.

The issue of NO_x emissions is a recurring problem in all scenarios. However, it is less critical in scenarios III and IV, where the higher presence of H_2 in the fuel allows for reaching higher dilution values that reduce these emissions below 1g/kWh. In this sense, NO_x emissions are a problem that is directly linked to the dilution degree used in engine operation, regardless of the level of H_2 in the fuel. Therefore, the three-way catalyst is the most feasible solution for scenarios I and II in order to meet emissions standards, necessitating stoichiometric combustion.

In later stages, it is possible to further increase dilution, which can significantly lower NO_x levels in the exhaust and improve thermal efficiency. However, limitations in the boosting system to achieve the required dilution rate or misalignments during engine transients suggest that the use of after-treatment systems, such as hydrogen-selective catalytic reduction devices, will continue to be required.

Finally, these findings illustrate a flexible roadmap that can be readjusted by the current regional situation, and which has the potential to significantly reduce the global warming footprint of transportation during the transition towards a hydrogen-based economy.

However, this study is based on very specific experiments that may not fully reflect the actual operation of a vehicle-mounted engine in certain circumstances. Therefore, further studies conducted under conditions closer to real driving conditions should be performed in subsequent research steps, in order to verify the attainability of the values indicated by the proposed method in more realistic situations.

List of abbreviations

AD	Anaerobic Digestion
AF_{st}	Stoichiometric Air-fuel Ratio
BEV	Battery Electric Vehicle
BTE	Brake Thermal Efficiency
BtL	Biomass-to-Liquid fuels
CA10	Combustion after 10% of fuel burnt
CA50	Combustion after 50% of fuel burnt
CA90	Combustion after 90% of fuel burnt
CAD	Crank Angle Degrees
CCS	Carbon Capture and Storage
CCV	Cycle-to-Cycle Variation
CFD	Computational Fluid Dynamics
CH_4	Methane
CLD	Cadmium Luminescence Detector
CNG	Compressed Natural Gas
CO	Carbon Monoxide
CO_2	Carbon Dioxide
COP21	Paris Climate Conference
COV_{IMEP}	IMEP covariace
DME	Dimethyl Ether
EGR	Exhaust Gas Recirculation
EPA	Environmental Protection Agency
EVC	Exhaust Valve Closing
EVO	Exhaust Valve Opening
EU	European Union
FID	Flame Ionization Detector
GIE	Gross Indicated Efficiency
GHG	Greenhouse Gases
H/C	Hydrogen-Carbon ratio
H_2	Hydrogen
H2-DI	Hydrogen Direct Injection
HC	Hydrocarbons
HCNG	Hydrogen-CNG fuel blends
HCNG1	HCNG blend with 1% in mass of H_2
HCNG2	HCNG blend with 2% in mass of H_2
HCNG3	HCNG blend with 3% in mass of H_2
HCNG25	HCNG blend with 25% in mass of H_2
HCNG50	HCNG blend with 50% in mass of H_2
HCNG75	HCNG blend with 75% in mass of H_2
HICE	Hydrogen Internal combustion Engine
HRR	Heat Release Rate
HVO	Hydrotreated Vegetable Oil
ICE	Internal Combustion Engine
IMEP	Indicated Mean Effective Pressure
ISCO	Indicated specific CO
$ISCO_2$	Indicated specific CO_2
ISHC	Indicated specific HC
$ISNO_x$	Indicated specific NO_x
IVO	Intake Valve Opening
IVC	Intake Valve Closing
LHV	Lower Heating Value
M	Molar mass
MBT	Maximum Brake Torque
N_2O	Dinitrogen Oxide
NDIR	Non-Dispersive Infrared Spectroscopy
NO_x	Nitrogen Oxides
O/C	Oxygen-Carbon ratio
O_2	Oxygen
OMEx	Oxymethylene Dimethyl Ethers
PFI	Port Fuel Injection
PM	Particulate Matter
PMA	Magneto-Pneumatic Analysis
RON	Research Octane Number
SI	Spark-ignition
SMR	Steam Methane Reforming
ST	Spark Timing
TCO	Total Cost of Ownership
X	Molar fraction
Y	Mass fraction

Funding

This research has been partially funded by FEDER and the Spanish Government through project RTI2018-102025-B-I00 (CLEAN-FUEL).

M. Olcina-Girona is partly supported by the grant CIACIF/2021/437 of the "Subvenciones para la contratación de personal investigador predoctoral (ACIF)" of the Conselleria d'Innovació, Universitats, Ciència i Societat Digital de la Generalitat Valenciana.

Funding for open access charge: CRUE-Universitat Politècnica de València.

CRediT authorship contribution statement

S. Molina: Project administration, Supervision. **R. Novella:** Project administration, Conceptualization, Supervision. **J. Gomez-Soriano:** Supervision, Formal analysis, Investigation, Writing – review & editing. **M. Olcina-Girona:** Methodology, Investigation, Formal analysis, Writing – original draft.

Declaration of competing interest

The authors declare that they have no known competing financial interests or personal relationships that could have appeared to influence the work reported in this paper.

Data availability

Data will be made available on request.

Acknowledgments

The authors wish to thank Mr. Gabriel Alcantarilla for his inestimable assistance during the experimental campaign.

References

[1] IPCC. Climate change 2021: The physical science basis. Contribution of working group I to the sixth assessment report of the intergovernmental panel on climate change [Masson-Delmotte, V., P. Zhai, A. Pirani, S. L. Connors, C. Péan, S. Berger, N. Caud, Y. Chen (eds.)]. Cambridge University Press, Cambridge, United Kingdom and New York, NY, USA; 2021, p. 3949. http://dx.doi.org/10.1017/9781009157896.002.

[2] Höhne N, Kuramochi T, Warnecke C, Röser F, Fekete H, Hagemann M, et al. The Paris Agreement: Resolving the inconsistency between global goals and national contributions. Climate Policy 2017;17(1):16–32. http://dx.doi.org/10.1080/14693062.2016.1218320.

[3] Ritchie H, Roser M. CO_2 and greenhouse gas emissions. 2020, Our World in Data, https://ourworldindata.org/co2-and-other-greenhouse-gas-emissions.

[4] Environment Agency G. Fact sheet: EU 2050 strategic vision "A Clean Planet for All" brief summary of the European commission proposal, no. December 2018. 2018.

[5] Burton T, Powers S, Burns C, Conway G, Leach F, Senecal K. A data-driven greenhouse gas emission rate analysis for vehicle comparisons. SAE Int J Electrified Veh 2023;12(1).

[6] Kim S, Kim J. Feasibility assessment of hydrogen-rich syngas spark-ignition engine for heavy-duty long-distance vehicle application. Energy Convers Manage 2022;252:115048. http://dx.doi.org/10.1016/j.enconman.2021.115048, URL https://www.sciencedirect.com/science/article/pii/S0196890421012243.

[7] Li F, Wang Z, Wang Y, Wang B. High-efficiency and clean combustion natural gas engines for vehicles. Automot Innov 2019;2(4):284–304. http://dx.doi.org/10.1007/s42154-019-00075-z.

[8] Lee U, Han J, Urgun Demirtas M, Wang M, Tao L. Lifecycle analysis of renewable natural gas and hydrocarbon fuels from wastewater treatment plants' sludge. 2016, http://dx.doi.org/10.2172/1327830, URL http://www.osti.gov/servlets/purl/1327830/.

[9] Jaro Jens MS. Market state and trends in renewable and low-carbon gases in Europe: A Gas for Climate report, no. December. European Biogas Association; 2021, URL https://www.europeanbiogas.eu/wp-content/uploads/2021/12/Gas-for-Climate-Market-State-and-Trends-report-2021.pdf.

[10] Muñoz P, Franceschini EA, Levitan D, Rodriguez CR, Humana T, Correa Perelmuter G. Comparative analysis of cost, emissions and fuel consumption of diesel, natural gas, electric and hydrogen urban buses. Energy Convers Manage 2022;257:115412. http://dx.doi.org/10.1016/j.enconman.2022.115412, URL https://www.sciencedirect.com/science/article/pii/S0196890422002084.

[11] Ji C, Hong C, Wang S, Xin G, Meng H, Yang J, et al. Evaluation of the variable valve timing strategy in a direct-injection hydrogen engine with the Miller cycle under lean conditions. Fuel 2023;343(October 2022):127932. http://dx.doi.org/10.1016/j.fuel.2023.127932.

[12] Yun H, Bu Z, Yang Z, Wang L, Zhang B. Optimization of fuel injection timing and ignition timing of hydrogen fueled SI engine based on DOE-MPGA. Int J Hydrogen Energy 2023;48(25):9462–73. http://dx.doi.org/10.1016/j.ijhydene.2022.12.068.

[13] Fuel Cells and Hydrogen Joint Undertaking (FCH). Hydrogen roadmap Europe. 2019, p. 70. http://dx.doi.org/10.2843/249013, URL https://fch.europa.eu.

[14] Serrano D, Laget O, Soleri D, Richard S, Douailler B, Ravet F, et al. Effects of methane/hydrogen blends on engine operation: Experimental and numerical investigation of different combustion modes. SAE Tech Pap 2010;3(2):223–43. http://dx.doi.org/10.4271/2010-01-2165.

[15] Duan H, Yin X, Kou H, Wang J, Zeng K, Ma F. Regression prediction of hydrogen enriched compressed natural gas (HCNG) engine performance based on improved particle swarm optimization back propagation neural network method (IMPSO-BPNN). Fuel 2023;331(P2):125872. http://dx.doi.org/10.1016/j.fuel.2022.125872.

[16] Du YL, Sun ZY, Huang Q, Sun YC. Observation study on the flame morphology of outwardly propagating turbulent HCNG-30 premixed flames. Int J Hydrogen Energy 2023;48(19):7096–114. http://dx.doi.org/10.1016/j.ijhydene.2022.04.007.

[17] Kosmadakis GM, Rakopoulos DC, Rakopoulos CD. Assessing the cyclic-variability of spark-ignition engine running on methane-hydrogen blends with high hydrogen contents of up to 50%. Int J Hydrogen Energy 2021;46(34):17955–68. http://dx.doi.org/10.1016/j.ijhydene.2021.02.158.

[18] Mehra RK, Duan H, Juknelevičius R, Ma F, Li J. Progress in hydrogen enriched compressed natural gas (HCNG) internal combustion engines - A comprehensive review. Renew Sustain Energy Rev 2017;80(May):1458–98. http://dx.doi.org/10.1016/j.rser.2017.05.061.

[19] Pandey V, Badruddin IA, Khan TM. Effect of H2 blends with compressed natural gas on emissions of SI engine having modified ignition timings. Fuel 2022;321(March):123930. http://dx.doi.org/10.1016/j.fuel.2022.123930.

[20] Oh S, Kim C, Lee Y, Park H, Lee J, Kim S, et al. Analysis of the exhaust hydrogen characteristics of high-compression ratio, ultra-lean, hydrogen spark-ignition engine using advanced regression algorithms. Appl Therm Eng 2022;215:119036. http://dx.doi.org/10.1016/j.applthermaleng.2022.119036, URL https://www.sciencedirect.com/science/article/pii/S135943112200970X.

[21] Gupta P, Tong D, Wang J, Zhuge W, Yan C, Wu Y, et al. Well-to-wheels total energy and GHG emissions of HCNG heavy-duty vehicles in China: Case of EEV qualified EURO 5 emissions scenario. Int J Hydrogen Energy 2020;45(15):8002–14. http://dx.doi.org/10.1016/j.ijhydene.2020.01.025.

[22] Sagar S, Agarwal AK. Knocking behavior and emission characteristics of a port fuel injected hydrogen enriched compressed natural gas fueled spark ignition engine. Appl Therm Eng 2018;141:42–50. http://dx.doi.org/10.1016/j.applthermaleng.2018.05.102, URL https://www.sciencedirect.com/science/article/pii/S1359431118310275.

[23] Park C, Lee S, Kim C, Choi Y. A comparative study of lean burn and exhaust gas recirculation in an HCNG-fueled heavy-duty engine. Int J Hydrogen Energy 2017;42(41):26094–101. http://dx.doi.org/10.1016/j.ijhydene.2017.08.170, URL https://www.sciencedirect.com/science/article/pii/S0360319917334730.

[24] Rao A, Liu Y, Ma F. Study of NOx emission for hydrogen enriched compressed natural along with exhaust gas recirculation in spark ignition engine by Zeldovich' mechanism, support vector machine and regression correlation. Fuel 2022;318(January):123577. http://dx.doi.org/10.1016/j.fuel.2022.123577.

[25] Rao A, Gao H, Ma F. Study of laminar burning speed and calibration coefficients of quasi-dimensional combustion model for hydrogen enriched compressed natural gas fueled internal combustion engine along with exhaust gas recirculation. Fuel 2021;283(x):119284. http://dx.doi.org/10.1016/j.fuel.2020.119284.

[26] Prasad RK, Agarwal AK. Experimental evaluation of laser ignited hydrogen enriched compressed natural gas fueled supercharged engine. Fuel 2021;289(October 2020):119788. http://dx.doi.org/10.1016/j.fuel.2020.119788.

[27] Yontar AA, Wong V. Influence of laser ignition on characteristics of an engine for hydrogen enriched CNG and iso-octane usage. Int J Hydrogen Energy 2021;46(74):37071–82. http://dx.doi.org/10.1016/j.ijhydene.2021.08.206.

[28] Molina S, Novella R, Gomez-soriano J, Olcina-girona M. Experimental evaluation of methane-hydrogen mixtures for enabling stable lean combustion in spark-ignition engines for automotive applications. SAE Tech Pap 2022;1–12. http://dx.doi.org/10.4271/2022-01-0471.Received.

[29] Molina S, Ruiz S, Gomez-Soriano J, Olcina-Girona M. Impact of hydrogen substitution for stable lean operation on spark ignition engines fueled by compressed natural gas. Results Eng 2023;17:100799.

[30] Payri F, Olmeda P, Martin J, Carreño R. A new tool to perform global energy balances in DI diesel engines. SAE Int J Eng 2014;7(1):43–59. http://dx.doi.org/10.4271/2014-01-0665.

[31] Benajes J, Olmeda P, Martín J, Carreño R. A new methodology for uncertainties characterization in combustion diagnosis and thermodynamic modelling. Appl Therm Eng 2014;71(1):389–99. http://dx.doi.org/10.1016/J.APPLTHERMALENG.2014.07.010.

[32] Pashchenko D. Thermochemical waste-heat recuperation as on-board hydrogen production technology. Int J Hydrogen Energy 2021;46(57):28961–8. http://dx.doi.org/10.1016/j.ijhydene.2020.11.108.

[33] Stefaan V, Roger S, Verhelst S. Technical paper for students and young engineers-. In: FISITA world automotive congress, Barcelona. 2004, p. 1–9.

[34] Shudo T, Nabetani S. Analysis of degree of constant volume and cooling loss in a hydrogen fuelled SI engine. SAE Tech Pap 2001;2(1). http://dx.doi.org/10.4271/2001-01-3561.

[35] Nieminen J, D'Souza N, Dincer I. Comparative combustion characteristics of gasoline and hydrogen fuelled ICEs. Int J Hydrogen Energy 2010;35(10):5114–23. http://dx.doi.org/10.1016/j.ijhydene.2009.08.098.

[36] Nieminen J, Dincer I. Comparative exergy analyses of gasoline and hydrogen fuelled ICEs. Int J Hydrogen Energy 2010;35(10):5124–32. http://dx.doi.org/10.1016/j.ijhydene.2009.09.003.

[37] Demuynck J, De Paepe M, Verhaert I, Verhelst S. Heat loss comparison between hydrogen, methane, gasoline and methanol in a spark-ignition internal combustion engine. Energy Procedia 2012;29:138–46. http://dx.doi.org/10.1016/j.egypro.2012.09.018.

[38] Ma F, Wang Y. Study on the extension of lean operation limit through hydrogen enrichment in a natural gas spark-ignition engine. Int J Hydrogen Energy 2008;33(4):1416–24. http://dx.doi.org/10.1016/j.ijhydene.2007.12.040.

[39] Li H, Karim GA, Sohrabi A. Examination of the oil combustion in a SI hydrogen engine. SAE Tech Pap 2004.

[40] Li H, Karim GA, Sohrabi A. Examination of the oil combustion in a S.I. Hydrogen engine. SAE Tech Pap 2004;(724). http://dx.doi.org/10.4271/2004-01-2916.